ELSEVIER

Available online at www.sciencedirect.com

SCIENCE DIRECT®

Applied Surface Science 214 (2003) 120–135

applied surface science

www.elsevier.com/locate/apsusc

A study of copper chemical mechanical polishing in urea–hydrogen peroxide slurry by electrochemical impedance spectroscopy

Tzu-Hsuan Tsai, Yung-Fu Wu, Shi-Chern Yen*

Department of Chemical Engineering, National Taiwan University, Taipei 106, Taiwan

Received 6 July 2002; received in revised form 6 July 2002; accepted 1 March 2003

Abstract

The electrochemical impedance spectroscopy (EIS) technique has been used to investigate the feasibility of urea–hydrogen peroxide (urea–H_2O_2) slurries in copper chemical mechanical polishing (Cu CMP). The performance of the inhibiting-type and the chelating-type additives, BTA and NH_4OH, were also explored. In order to analyze the surface-reaction characteristics of Cu, the equivalent circuit of double capacitor mode was mainly used to simulate the corrosion behaviors of Cu CMP in various slurries. In addition, via measuring dc potentiodynamic curves and open circuit potential (OCP), the corrosion characteristics were obtained in various slurries. Both EIS and AFM experimental results indicate that the slurry composed of 5 wt.% urea–H_2O_2 + 0.1 wt.% BTA + 1 wt.% NH_4OH can achieve the better Cu CMP performance. Its rms-roughness (R_q) after CMP and the removal rate (RR) attain to 2.636 nm and 552.49 nm/min, respectively.
© 2003 Elsevier Science B.V. All rights reserved.

Keywords: Copper; Chemical mechanical polishing; Urea–hydrogen peroxide slurry; Electrochemical impedance spectroscopy; Potentiodynamic curve

1. Introduction

Copper chemical mechanical polishing (Cu CMP) has been employed as the key planarization technique to delineate conductive interconnects in the ultra large-scale integrated circuit (ULSI) manufacturers [1]. Although the basic principles of dielectric CMP have been investigated and understood, the mechanisms of metal CMP remain greatly complicated and different from the dielectric CMP. The metal takes the plastic deformation more easily [2] and is more sensitive to corrosion during CMP. The model proposed by Kaufman et al. [3] indicates that the metal planarization during CMP is a result of repeated processes of film formation, film removal and re-passivation in the slurry. And this mechanism has been applied to explain the CMP processes for Cu planarization [4]. As indicated from this mechanism, the passivation of the metal surface and the dissolution of the abraded materials become the important functions of Cu CMP slurry. To achieve slurry formulation that could successfully planarize Cu damascene structures, several requirements had to be met: sufficiently high and uniform Cu removal rates, good metal to dielectric selectivity, minimal dishing and low defects, and ease to use [5,6].

* Corresponding author. Tel.: +886-2236-30397; fax: +886-2236-30397.
E-mail address: scyen@ntu.edu.tw (S.-C. Yen).

0169-4332/03/$ – see front matter © 2003 Elsevier Science B.V. All rights reserved.
doi:10.1016/S0169-4332(03)00272-1

A commonly used CMP process utilizes abrasive particles suspended in the colloid slurry. Also, different additives or reagents can be combined with the slurry to achieve the above requirements. For examples, an oxidizing agent can be used to form a native passive film on metal during CMP [7–9]. Some materials, such as chelating agents or dispersing agents, can also be combined with the slurry to improve the dissolution-ability and the transport-property of the slurry [10–12], and still others, such as benzotriazole (BTA) or carboxylic acid, can be added to inhibit the corrosion of the surface being polished [13,14]. In prior researches, the oxidizing-type reagent containing metal ions is often used for CMP slurry [7,8]. However, an issue of these metal ion-based reagents is that metal ions would contaminate the exposed surface of the semiconductor wafer [15]. Consequently, oxidizing agents containing metal ions could affect the reliability and functionality of semiconductor devices on the wafer.

In another researches still, slurry compositions for Cu CMP have principally employed hydrogen peroxide (H_2O_2) as an oxidizing agent [9]. As H_2O_2 has several advantages, including no metal-ion contamination, non-highly acidic or alkaline components and with the high oxidizing ability. Nevertheless, H_2O_2 decomposes to H_2O and O_2 easily to worsen the stability of the slurry and cause slurry delivery problems. Furthermore, properties of the H_2O_2 slurry are altered with ease by additives and results in the low reliable application for CMP [16]. Thus, there is a need to achieve a slurry formulation so that Cu CMP processing can become practical.

Herein, urea–hydrogen peroxide (urea–H_2O_2) is adopted as the oxidant of Cu CMP slurry. As urea–H_2O_2 is verified experimentally more stable than H_2O_2 alone and it can be predicted that the additives, such as inhibitors, organic acids, surfactants or chelating agents, are more compatible and stable in urea–H_2O_2 system than in H_2O_2 system. The purpose of this research was to investigate the chemical and mechanical effects of the additives on Cu CMP in urea–H_2O_2 slurry.

In this study, the effects of various chemical components were primarily analyzed by the electrochemical impedance spectroscopy (EIS). The EIS is a suitable ac technique to characterize the corrosion or the passivation of metal film, while the dc technique might accelerate the polarization and destabilize the passivation [17]. The CMP slurry often contains dilute electrolyte due to the low-level contaminant limit in IC processing. As a result, solution resistance often makes dc experiments difficult to perform accurately. Thus, we introduce the EIS method to eliminate this error in dilute solution. Herein, the response of corroding Cu electrodes to small-amplitude alternating potential signals of widely varying frequency has been analyzed. The time-dependent current response $I(t)$ of an electrode surface to a sinusoidal alternating potential signal $V(t)$ can be expressed as an angular frequency (ω) dependent impedance $Z(\omega)$, where $V(t) = V_0 \sin \omega t$, $I(t) = I_0 \sin(\omega t + \phi)$ and $Z(\omega) = V(t)/I(t)$. Various processes at the surface absorb electrical energy at discrete frequencies, causing a time lag and a measurable phase angle, ϕ, between the time-dependent excitation and response signals. All of these processes can be simulated from resistive–capacitive electrical networks. As a result, EIS can determine in principle a number of fundamental parameters relating to electrochemical kinetics and has been the subject of vigorous research. Also, the EIS method can characterize the passive-film quality and monitor the Cu CMP performance. Although electrochemical behaviors of Al CMP have been studies using the EIS technique [18], little research has been done on Cu CMP.

Still the dc potentiodynamic curves and open circuit potential (OCP) were used here to evaluate the corrosion kinetics of Cu. Furthermore, the passive film and the surface quality of Cu were analyzed by use of X-ray diffraction (XRD) technique and atomic force microscopy (AFM). The research may provide better understanding of electrochemical behaviors of Cu CMP and effects of the additives in urea–H_2O_2 slurry.

2. Experimental

Commercial pure Cu sheets with 0.3 mm thickness were diced into dimension of 1 cm × 1 cm samples for electrochemical measurements, including electrochemical impedance spectroscopy (EIS), open circuit potential (OCP) and dc potentiodynamic curves. In addition, Cu was punched to disk of 3 in. in diameter for polishing experiments to obtain its surface analysis and morphology. All specimens were prior to be degreased by the cathode electrochemical method at

6 V for 20 s, and then were cleaned in 3 wt.% H_2SO_4 solution for 3 min by use of an ultrasonic bath to remove the surface oxide. Further the samples were dried in nitrogen gas and transferred to the electrochemical measuring or polishing experiments. To investigate the effects of additives on Cu in urea–H_2O_2, the slurries were prepared by using analytical grade reagents, including urea–H_2O_2, BTA and NH_4OH all with 5 wt.% α-alumna abrasive of about 50 nm in size.

The electrochemical test cell was composed of the Cu working electrode, the platinum counter electrode and the Ag/AgCl reference electrode with a Luggin probe. The downward force and the rotating speeds under Cu abrasion was 5 psi and 100 rpm applied by a rotating motor above the test cell, and then the pressure was modulated by use of a weighing balance below the entire test cell. EIS measurements were performed with Solartron FRA 1260 and 1286 electrochemical interface system and operated over the frequency range from 10^4 to 10^{-2} Hz at OCP. A small amplitude perturbation of 10 mV in a sine wave was applied to ensure the linearity for impedance analysis. In addition, the dc electrochemical experiments were conducted by use of a potentiostat/galvanostat of EG&G Model 273, while the corrosion software of EG&G Model 352 was adopted for electrochemical calculations. The dc potentiodynamic curves with a voltage scan rate of 5 mV/s were used to measure the corrosion current densities and potential. Meanwhile, the corrosion current density was converted to the corresponding corrosion rate (CR, nm/min) according to Faraday's law [19]. Data of OCP versus time were also obtained by above potentiostat of EG&G Model 273. The specimen was first anodized in the testing solution at +500 mV (versus Ag/AgCl) to form a higher oxidizing state of Cu surface until the system achieved the steady-state current density. This pre-treatment took within about 10 min for Cu in various slurries. After the anodizing of Cu, the variation in OCP over the surface state of polishing or pressure releasing was recorded.

For polishing experiments, a Lapmaster LM-51 polisher operating at 80/60 rpm of the platen/carrier rotating speeds, respectively, and 5 psi were used with the polishing pad of IC 1000/SUBA IV supplied by Rodel. Before CMP, the slurry must be stirred with high stress in a mixer to maintain the slurry suspension for the test period. During CMP, the slurry was delivered between Cu and the pad with the flow rate of 100 ml/min. The removal rate (RR) was calculated from the weight loss of Cu sheets before and after polishing for 3 min and the values were obtained by averaging over three tests.

The passive films existed on the Cu surface were distinguished by X-ray diffraction (XRD) recorded from 10 to 60° 2θ. Atomic force microscope (AFM) with tapping mode was used to characterize the surface morphology and roughness before and after CMP. The rms-roughness (R_q) was adopted to compare the surface quality, calculated by the software package, and it is defined as

$$R_q = \sqrt{\frac{\sum_{i=1}^{n}(Z_i - \bar{Z})^2}{n}}$$

where Z_i is the height values of single data points in the image; $\bar{Z}$, the mean value of all height values in the image; and n, the number of data points within the image.

3. Results and discussion

3.1. Oxidation effect of urea–H_2O_2 on Cu

Fig. 1 shows the variation in the relative open circuit potential (ΔE) of Cu films with the change of surface state. In this figure, ΔE represents the change of OCP from its initial value. Before measuring OCP, Cu samples were forced to a higher oxidation state in the testing slurry by pre-polarizing. Then a polishing force with 5 psi and 100 rpm was applied on the sample. As soon as the mechanical force was exerted, OCP decreased abruptly (see Fig. 1) indicating the exposure of the active Cu surface. At about 310 s, the mechanical action was released for a period so that OCP increased due to the re-passivation of the fresh Cu. In this period, urea–H_2O_2 concentrations had a clear effect on increasing OCP. It has been found that a higher urea–H_2O_2 concentration would bring a larger increase in OCP, i.e. the faster oxidizing rate. Mechanical polishing with 5 psi and 100 rpm was then reapplied at 530 s, and OCP dropped again to the active level of Cu. These data indicate that an abradable layer was continuously formed by the oxidization of urea–H_2O_2 on the Cu surface. The abradable layer was then removed in a controlled manner by mechanical action.

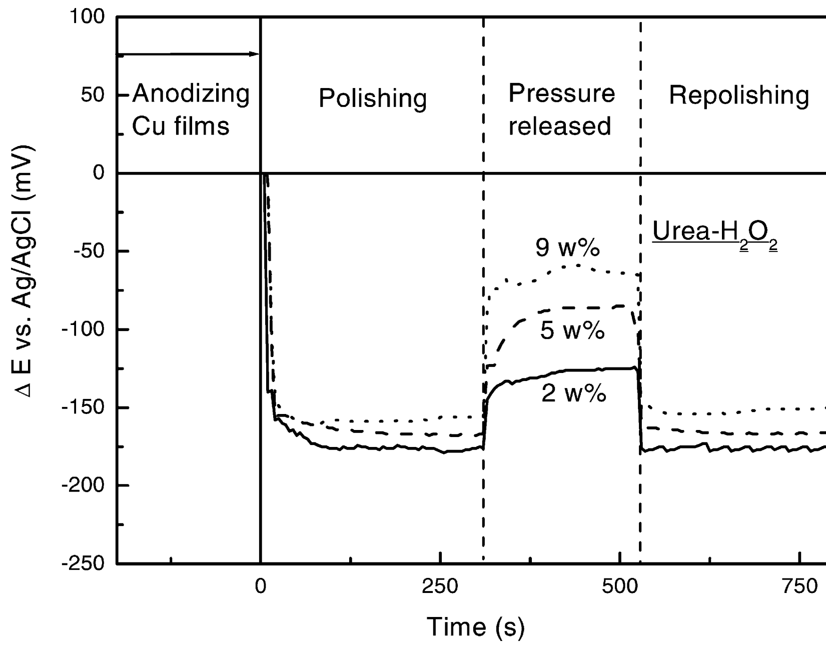

Fig. 1. Variation of OCP with time in the slurry of the different urea–H_2O_2 concentrations with either pressure released or polishing at 5 psi and 100 rpm.

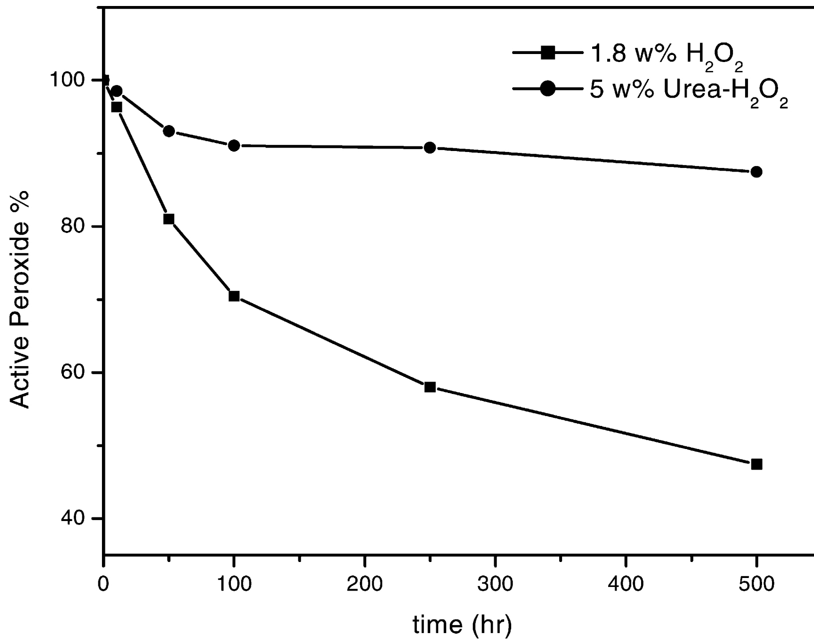

Fig. 2. Active peroxide percentage of H_2O_2 and urea–H_2O_2 slurries as a function of time.

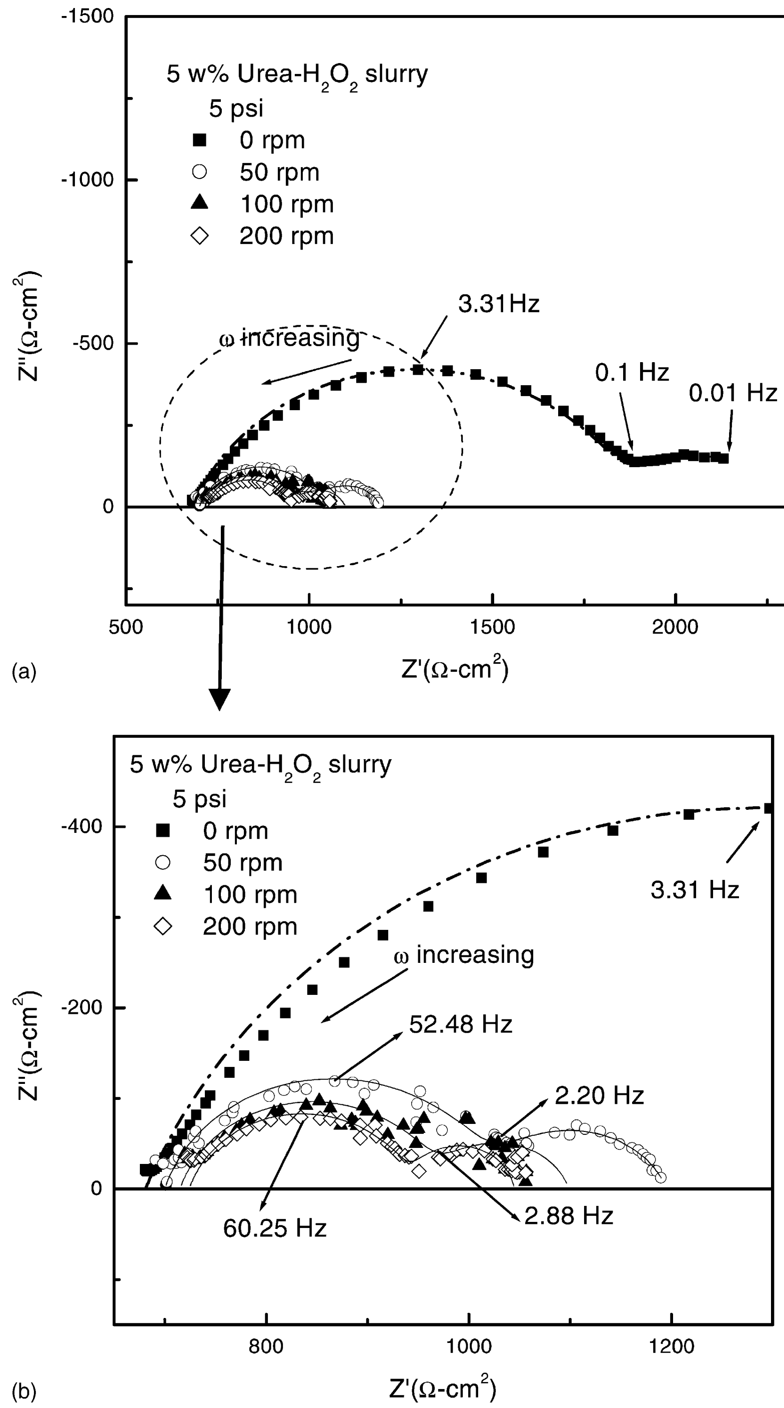

Fig. 3. Effect of rotating speeds on Nyquist plots for copper in 5 wt.% urea–H_2O_2 slurry at a constant pressure of 5 psi.

Once the mechanical polishing has stopped, a passive film would remains on the surface to control the proceeding corrosion.

On the other hand, in order to compare the stability of urea–H_2O_2 slurry with H_2O_2 slurry, 5 wt.% urea–H_2O_2, corresponding to about 1.8 wt.% H_2O_2, and 1.8 wt.% H_2O_2 slurries were periodically analyzed for titration with potassium permanganate to determine the activity of the peroxide. As Fig. 2 shows, percentage of the active peroxide appears to degrade at a faster rate than the slurry including urea–H_2O_2. This drop in active percentage might be due to the spontaneous decomposition of H_2O_2. Therefore, urea–H_2O_2 is the more preferred oxidizer than H_2O_2.

3.2. Mechanical effect

Herein, EIS measurement was introduced to analyze the mechanical effect of various rotating speeds on Cu CMP in 5 wt.% urea–H_2O_2 slurry. Nyquist plots and Bode plots display the EIS results in Figs. 3 and 4, respectively. As shown in Fig. 3, the experimental result of Nyquist plots for Cu in urea–H_2O_2 slurry exhibits a double-semicircle mode with increasing frequency in a counter-clockwise direction. Moreover, Bode plot of Fig. 4(b) also shows two maximum peaks at intermediate frequency, which indicate the presence of two time lags. Therefore, a double-capacitance mode is used to fit these EIS data of Cu–slurry interface. The equivalent circuit simulating the interface behavior of Cu CMP is depicted in Fig. 5,where R_s is the solution resistance; R_{pf}, the passive-film resistance; R_{ct}, the charge-transfer resistance; C_{pf}, the passive-film capacitance; and C_{dl}, the double-layer capacitance. While the resistive elements provide the real of impedance, i.e. $Z_R = R$, the two capacitive elements produce imaginary components, i.e. $Z_C = -j/\omega C$ and a double-semicircle mode is induced. However, in the case of a non-uniform surface with distributed elements, the ideal capacitive element would be replaced by the constant-phase element (CPE), and then the EIS results of the practical electrodes could be fitted more agreeably. Relevant results to surface conditions are discussed in Section 4.

The simulated results were plotted with the solid lines in Figs. 3 and 4. As shown in Fig. 3(a) and (b), the static sample (with 0 rpm) had a broader range of impedance in comparison with the polished samples. It seems that the polishing action may affect the surface characteristics drastically in 5 wt.% urea–H_2O_2 slurries. According to the theoretical deduction, the imaginary component disappears, leaving only the resistance at very high or low frequency. The impedance modulus approaches R_s at high frequency end of Bode plot, while it is equal to the sum of R_s, R_{pf} and R_{ct} at low-frequency end. As shown in high-frequency region of Fig. 4(a), R_s increased from 680 to 724 Ω cm^2 with an increase in rotating speeds. It is due to a shorter staying time for the slurry between the metal and polishing pad under a higher rotating speed, and the larger R_s was then caused. After the exclusion of R_s from the low-frequency impedance, $R_{pf} + R_{ct}$ could reveal. As Fig. 4(a) shows the polishing action brought $R_{pf} + R_{ct}$ lower in comparison with the static one. This decrease in $R_{pf} + R_{ct}$ is associated with the removal of passive film. For the static sample, the passive film formed on Cu surface and thus a higher passive-film resistance, 1215 Ω cm^2, was induced. Meantime, the passive film would block the oxidation of Cu, so that the charge-transfer resistance was also larger and the fitted value was 332 Ω cm^2.

For the sample with 50 rpm polishing, the passive film could be removed by the polishing action. Hence, the fitted value of R_{pf} decreased to 328 Ω cm^2 substantially due to a thinning passive film. In addition, the oxidation could proceed more easily because of some fresh Cu surfaces exposed in 5 wt.% urea–H_2O_2 slurry, and then R_{ct} decreased to 168 Ω cm^2. Similarly, for the larger polishing action, such as 100 or 200 rpm, the low-frequency impedances show further lower $R_{pf} + R_{ct}$, induced by the thinner passive film. In general, the EIS measurement and simulation can provide better understanding of the mechanical action in urea–H_2O_2 slurry for Cu CMP process.

3.3. Chemical effect

The effects of chemical components on Cu CMP in urea–H_2O_2 slurries are studied as following. Since the oxidizing ability of urea–H_2O_2 for Cu has been discussed earlier, the actions of the inhibiting-type and the chelating-type additives are investigated herein. First, BTA was added into the urea–H_2O_2 slurry because it is a well-known corrosion inhibitor usually

used in electronic industry [20]. During Cu CMP, it is expected that an inhibiting-type additive may slow down the isotropic corrosion rate of Cu, and then bring a further planarization. The EIS of Cu in 5 wt.% urea–H_2O_2 + 0.1 wt.% BTA slurries was measured and shown in Fig. 6. Meanwhile, the inhibiting action of BTA on Cu depending on different immersion periods was discussed. As Fig. 6(a) shows, all the

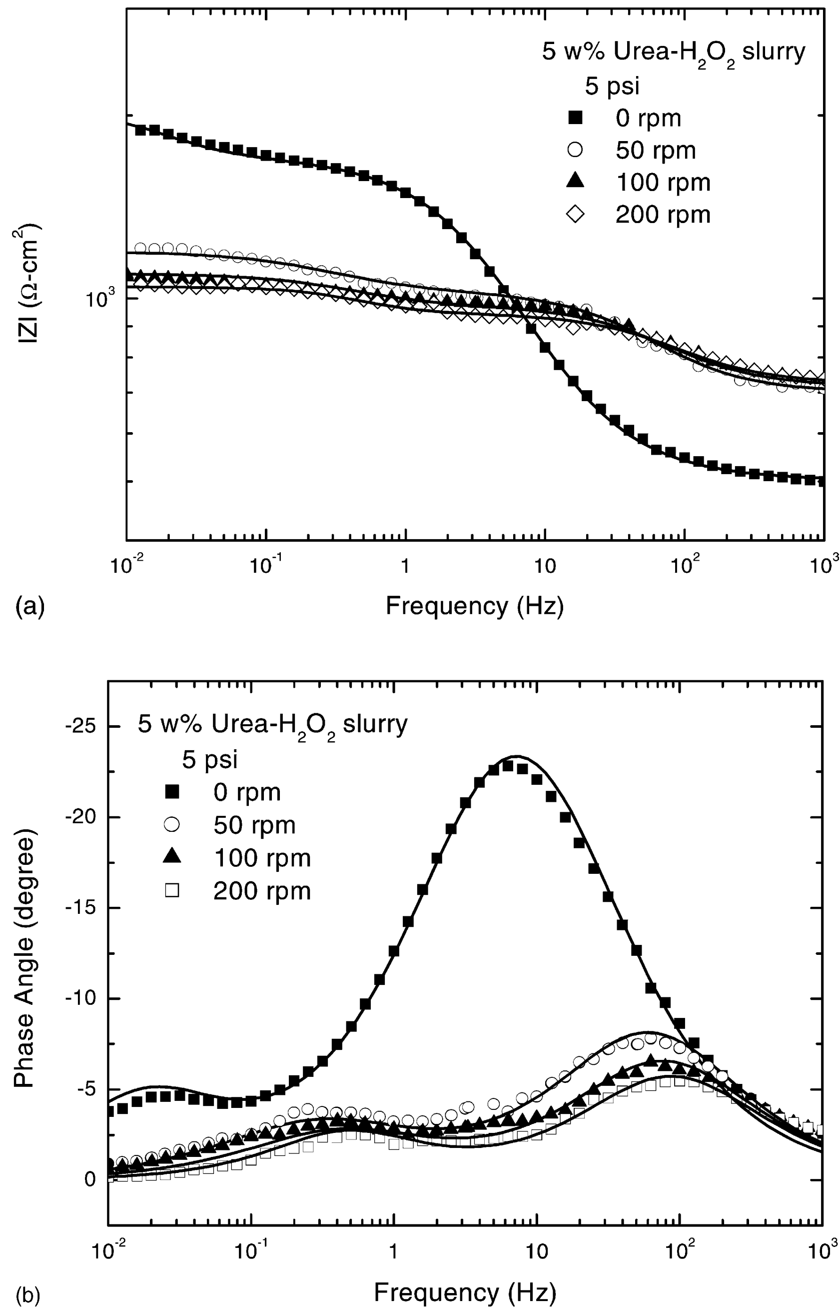

Fig. 4. Effect of rotating speeds on Bode plots for copper in 5 wt.% urea–H_2O_2 slurry at a constant pressure of 5 psi.

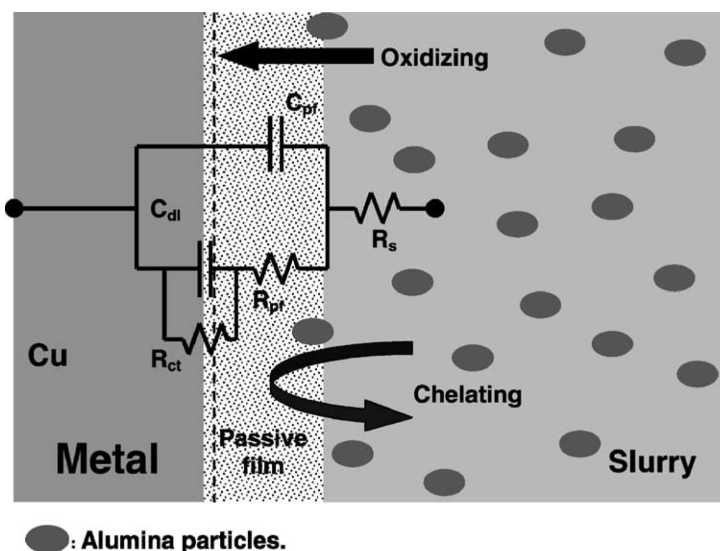

Fig. 5. Equivalent circuit diagram and electrochemical characteristics used to fit the EIS results of copper CMP in urea–H_2O_2-based slurries.

low-frequency impedances are above $10^4\ \Omega\ cm^2$, and these values are one order of magnitude more than those without BTA, as shown in Fig. 4(a). Moreover, the low-frequency impedance increased with immersion time. It seems that the inhibiting action of BTA was not achieved completely until the overall Cu surface was adsorbed. Still as shown in the phase angle–frequency diagram of Fig. 6(b), only one peak exits and the other peak disappears. These phenomena and all indicate that the adsorption of BTA may even inhibit the formation of passive film on Cu. According to above deduction, the equivalent circuit of Fig. 5 is simplified by neglecting the passive-film elements, R_{pf} and C_{pf}, and is used to simulate the EIS data of Cu CMP in 5 wt.% urea–H_2O_2 + 0.1 wt.% BTA slurry. The solid lines in Fig. 6 represent the fitting with the simplified equivalent circuit. The results show that the simplified equivalent circuit well exhibits the electrochemical nature of Cu CMP. As Fig. 6(a) shows, the low-frequency impedance decreased apparently after 1 min polishing, and the phase angle had a smaller peak shift toward the higher frequency than those without polishing. It reveals that the adsorption layer of BTA, instead of the native oxide of Cu, would become an abradable material for the Cu CMP process, herein.

Fig. 7 shows the dc potentiodynamic curves of Cu in urea–H_2O_2 slurries. The BTA adding and abrasion effects are clear by comparing their corrosion parameters of Cu, including corrosion current densities (i_{corr}) and potential (E_{corr}). Based on the dc potentiodynamic curves obtained, the corrosion–potential drop caused by polishing (ΔE_d), the removal rate (RR) and the corrosion rate (CR) of Cu were calculated and all of the corrosion parameters are listed in Table 1. As shown in Fig. 7, it had an obvious potential drop after polishing (ΔE_d) in 5 wt.% urea–H_2O_2 slurry. This represents the Cu surface could be protected by its native oxide before polishing, and this oxide is abradable. As a result, polishing action led to the more active corrosion potential and the larger anodic current density. The corresponding corrosion rate was 2.92 nm/min listed in Table 1. As 0.1 wt.% BTA was added into 5 wt.% urea–H_2O_2 slurry, the corrosion potential would remain at a noble state due to the inhibiting action of the BTA adsorption-layer. The corrosion current density of Cu, however, was the lowest, about three orders of magnitude less than that in 5 wt.% urea–H_2O_2 slurry without adding BTA. Afterwards, a mechanical polishing action was exerted and the BTA adsorption-layer was destroyed locally. Consequently, Cu could be corroded in a lower potential, and still the corrosion rate was very low, about 0.012 nm/min.

From above EIS results and dc potentiodynamic curves, the protective capability of BTA can be seen

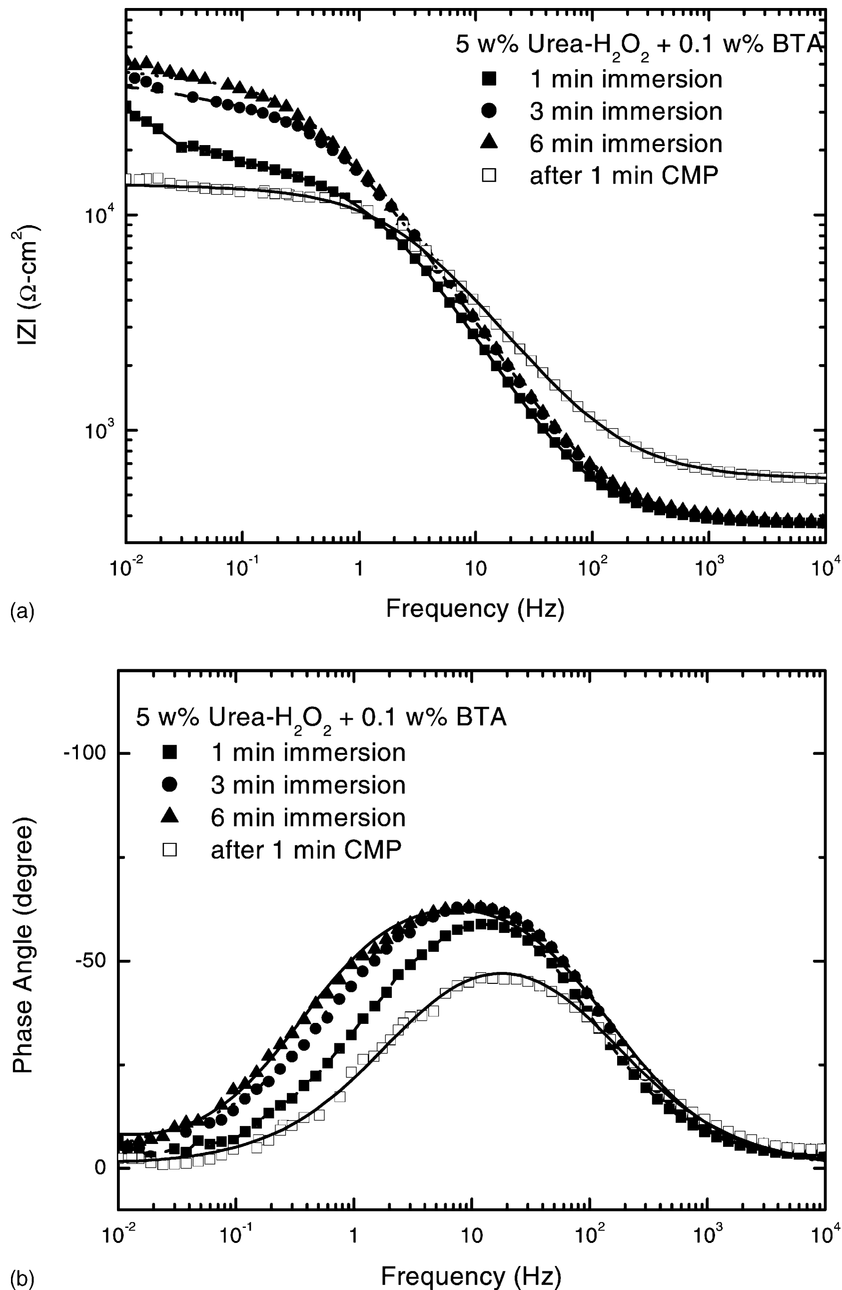

Fig. 6. Effects of the immersion time and CMP on Bode plots for copper in 5 wt.% urea–H_2O_2 + 0.1 wt.% BTA slurry (CMP: at 5 psi and 100 rpm).

and this adsorbed layer is more useful than the porous oxide for inhibiting corrosion of the region with lower-strength mechanical action. Hence, the damage of Cu lines can be prevented. However, the existence of the native oxide for Cu CMP is necessary. Polishing oxide, instead of polishing Cu, can avoid the plastic deformation and dislocation of Cu structures induced by the direct removal of metal. Furthermore, the

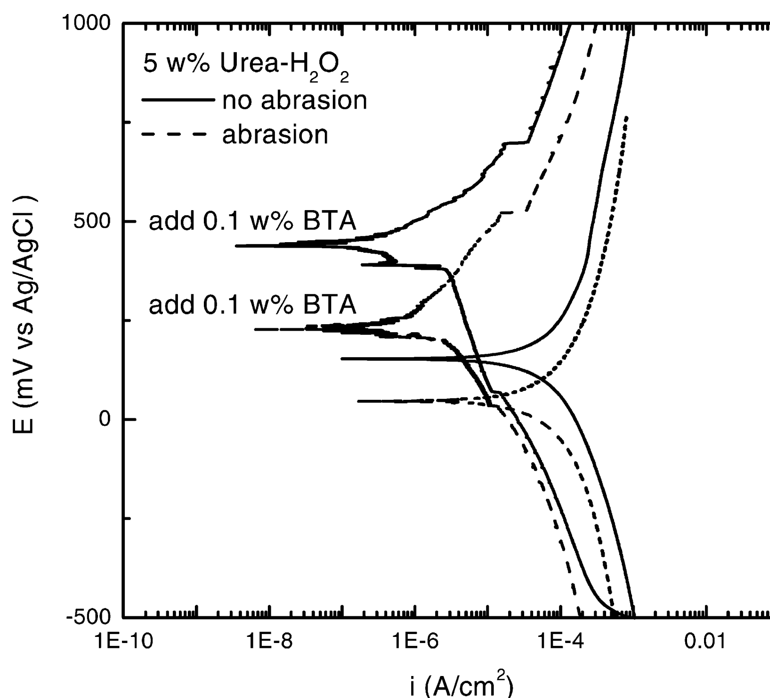

Fig. 7. Effects of abrasion and the addition of BTA on the potentiodynamic curves for copper in 5 wt.% urea–H_2O_2 slurry (abrasion: at 5 psi and 100 rpm).

removal rates of Cu in 5 wt.% urea–H_2O_2 slurries with and without 0.1 wt.% BTA were low, 341.16 and 472.63 nm/min, respectively. Thus, another appropriate additive is required to accelerate the oxidation of Cu and to remove the passive film rapidly.

Herein, NH_4OH is considered to add into urea–H_2O_2 slurries for its excellent chelating ability with Cu or its compounds, and its alkaline property is appropriate for the formation of the native oxide of Cu according to Pourbaix diagram [21]. The dc potentiodynamic curves of Cu in 5 wt.% urea–H_2O_2 + 1 wt.% NH_4OH slurries are shown in Fig. 8, and the corrosion parameters are listed in Table 1. It indicates that the corrosion potential of Cu was lower in NH_4OH-containing slurries, and even lay in a negative. That is, a spontaneous corrosion takes place.

Table 1
Summary of potentiodynamic parameters, corrosion rates (CR) and removal rates (RR) of copper in various slurries

Slurry	pH	No abrasion		Abrasion		ΔE_d (mV)	RR (nm/min)	CR[a] (nm/min)
		E_{corr} (mV)	i_{corr} (A/cm^2)	E_{corr} (mV)	i_{corr} (A/cm^2)			
5 wt.% urea–H_2O_2	4.63	152.91	1.13×10^{-4}	46.21	1.33×10^{-4}	106.70	472.63	2.92
5 wt.% urea–H_2O_2 + 0.1 wt.% BTA	4.60	452.12	4.32×10^{-7}	239.02	5.41×10^{-7}	213.10	341.16	0.012
5 wt.% urea–H_2O_2 + 1 wt.% NH_4OH	10.62	−216.28	3.86×10^{-4}	−218.83	1.48×10^{-3}	2.55	649.73	32.57
5 wt.% urea–H_2O_2 + 0.1 wt.% BTA + 1 wt.% NH_4OH	10.49	−155.11	4.91×10^{-6}	−166.76	1.90×10^{-4}	11.65	552.49	4.18

[a] Corrosion rates (CR) corresponding to the corrosion current densities of abrasion are calculated using Faraday's law.

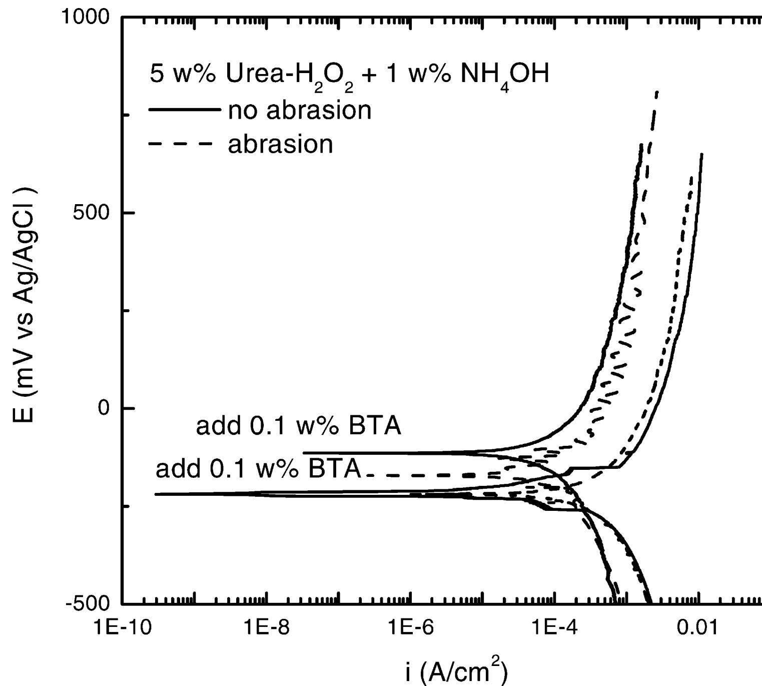

Fig. 8. Effects of abrasion and the addition of BTA on the potentiodynamic curves for copper in 5 wt.% urea–H_2O_2 + 1 wt.% NH_4OH slurry (abrasion: at 5 psi and 100 rpm).

Data also show that a larger corrosion current density was obtained in 5 wt.% urea–H_2O_2 slurry by adding 1 wt.% NH_4OH.

Unlike the urea–H_2O_2 slurry without adding NH_4OH, the ΔE_d was ambiguous for the NH_4OH containing slurry. As summarized in Table 1, ΔE_d of Cu in 5 wt.% urea–H_2O_2 decreased from the largest of only BTA adding, 213.10 mV, to the smallest of only NH_4OH adding, 2.55 mV. This is because NH_4OH acts not only as an oxidizing enhancer due to its alkaline property, but also as a strong chelating ligand due to the high stable–constant of coordination with Cu and compounds thereof [22]. So, the re-passivation of Cu surface is followed unceasingly by the sequence of mechanical removal of the passive film and dissolution of the abraded oxide. As listed in Table 1, the corrosion rate in 5 wt.% urea–H_2O_2 + 1 wt.% NH_4OH slurry, 32.57 nm/min, is so high that this slurry would not meet the requirement of global planarization even though it has the highest removal rate of Cu, 649.73 nm/min, among the slurries. Consequently, adding both the inhibiting- and the chelating-type additives into urea–H_2O_2 slurries might be predicted a better CMP performance. As can be seen in Fig. 8, the potential drop (ΔE_d) increased and the corrosion current density decreased when 0.1 wt.% BTA was added. It indicates that the inhibiting action of BTA would decrease the corrosion rate even though adding NH_4OH induces the stronger oxidation and dissolution actions. The removal rate of Cu in 5 wt.% urea–H_2O_2 + 0.1 wt.% BTA + 1 wt.% NH_4OH slurry, 552 nm/min, was higher than that in the slurry without adding NH_4OH. Therefore, better compromise between protection and dissolution can be achieved and further CMP efficiency can be accomplished.

Fig. 9 shows the EIS results of Cu in 5 wt.% urea–H_2O_2 + 1 wt.% NH_4OH slurries. The phase angle seems to have very small change with immersion time in 5 wt.% urea–H_2O_2 + 1 wt.% NH_4OH system. Meantime, the equivalent circuit of Fig. 5 is adopted to simulate the EIS results in spite of the unobserved peak at 0.1–1 Hz in the slurry without adding BTA. Table 2 presents the simulated results. It reveals that

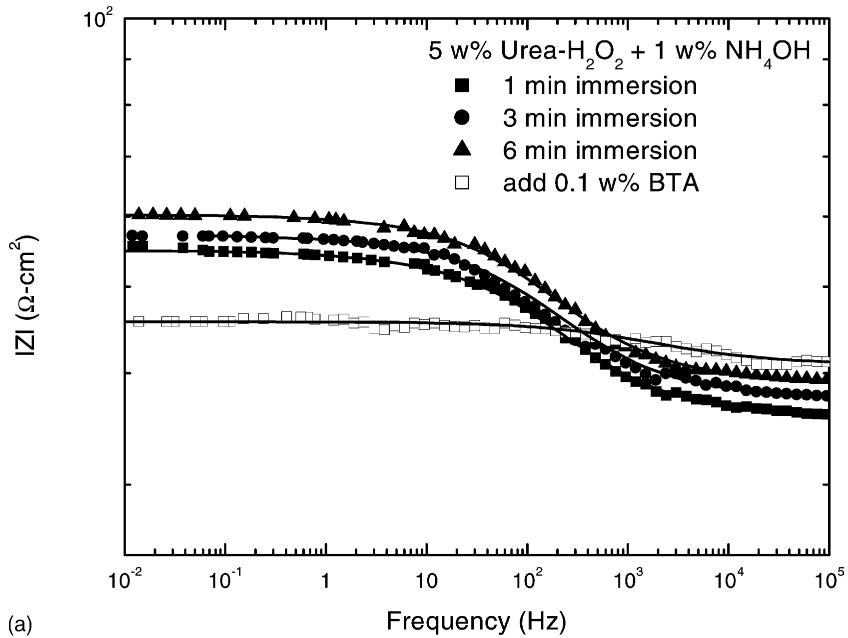

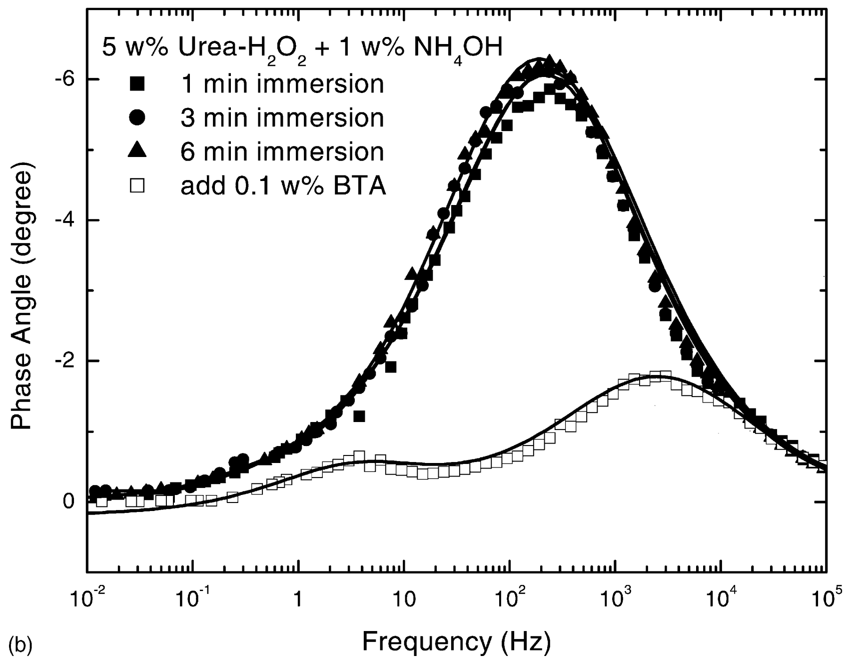

Fig. 9. Effects of the immersion time and the addition of BTA on Bode plots for copper in 5 wt.% urea–H_2O_2 + 1 wt.% NH_4OH slurry.

Table 2
Values of R_s, R_{pf} and R_{ct} for copper in 5 wt.% urea–H_2O_2 + 1 wt.% NH_4OH solution determined from EIS of Fig. 9 and simulated by the equivalent circuit of Fig. 5

Treatment	5 wt.% Urea–H_2O_2 + 1 wt.% NH_4OH		
	R_s (Ω cm^2)	R_{pf} (Ω cm^2)	R_{ct} (Ω cm^2)
Immersion 1 min	35.96	18.61	0.59
Immersion 3 min	37.71	19.32	0.34
Immersion 6 min	39.31	19.13	0.01
Adding 0.1 wt.% BTA	40.18	3.84	3.78

the R_{ct} is low but remains the similar value in spite of the longer immersion time. In this slurry, the Cu surface appears to be oxidized rapidly and dissolved quickly by NH_3 at the same time. As a result, a steady resistance of the passive film, R_{pf}, was caused. Moreover, its fitted value in the NH_4OH-containing slurry was much smaller than those in only urea–H_2O_2-containing slurry by comparing the Fig. 9 with Fig. 4. In other words, adding NH_4OH enhances the dissolution action, and thus a higher oxidization and removal rate may be achieved. As mentioned earlier, BTA can inhibit the corrosion action of Cu CMP effectively. Indeed, the relation between phase angle and frequency underwent a different change once 0.1 wt.% BTA was added into the 5 wt.% urea–H_2O_2 + 1 wt.% NH_4OH slurry. As presented in Table 2, the increased R_{ct} seems to represent a slower oxidation on Cu surface, and then a smaller R_{pf} was induced. These EIS results are consistent with the discussion of dc potentiodynamic curves.

Fig. 10 presents the X-ray diffraction (XRD) analysis of Cu in 5 wt.% urea–H_2O_2 + 0.1 wt.% BTA + 1 wt.% NH_4OH slurry. It depicts the XRD patterns recorded from 10 to 60° of 2θ for Cu films. The XRD patterns for the Cu before polishing only shows the reflections $d_{(1\ 1\ 1)}$ ($2\theta = 43.32°$) and $d_{(2\ 0\ 0)}$ ($2\theta = 50.47°$) corresponding to metallic Cu. When Cu was dipped in this slurry for 5 min, in addition to metallic Cu peaks, shows the diffraction maximum ($2\theta = 36.78°$), labeled p, corresponding to Cu_2O, $d_{(1\ 1\ 1)}$, in the XRD pattern of Fig. 10. However, the peak resulted from Cu_2O would disappear after polishing. It indicates that the performance of Cu CMP in 5 wt.% urea–H_2O_2 + 0.1 wt.% BTA + 1 wt.% NH_4OH slurry did obey the repeated processes

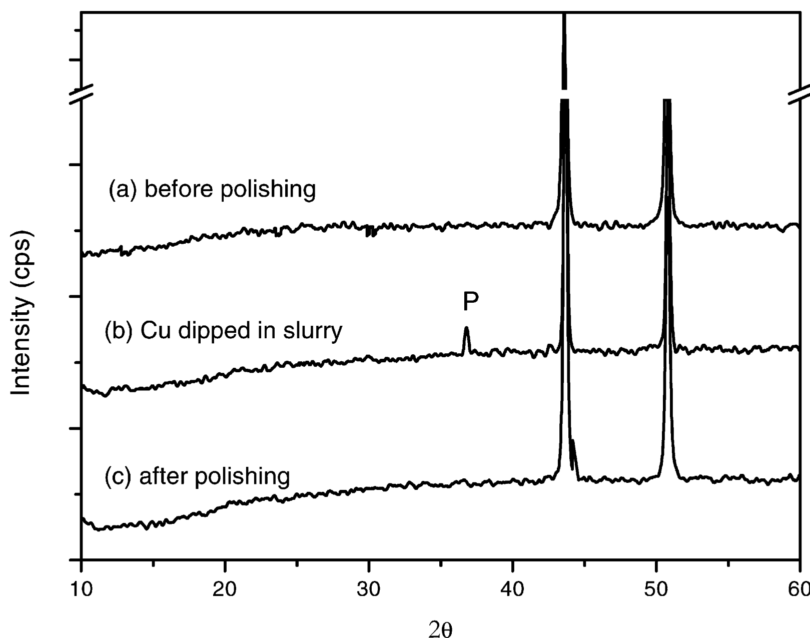

Fig. 10. The XRD patterns for copper in 5 wt.% urea–H_2O_2 + 0.1 wt.% BTA + 1 wt.% NH_4OH slurry: (a) before CMP, (b) dipping for 5 min, and (c) after CMP.

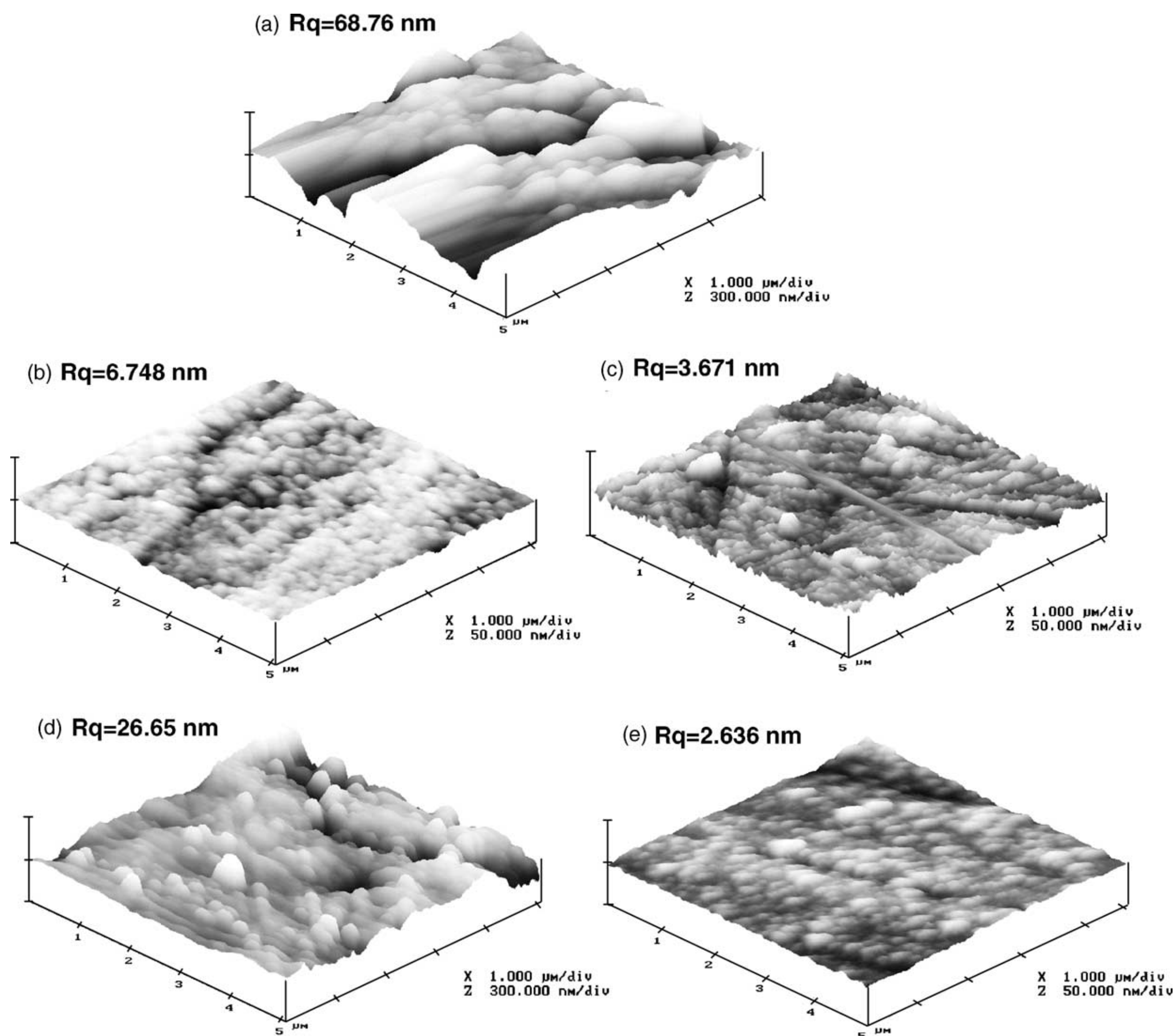

Fig. 11. AFM micrographs and the surface roughness of copper surface: (a) before polishing and (b)–(e) after CMP ((b) 5 wt.% urea–H_2O_2; (c) 5 wt.% urea–H_2O_2 + 0.1 wt.% BTA; (d) 5 wt.% urea–H_2O_2 + 1 wt.% NH_4OH; and (e) 5 wt.% urea–H_2O_2 + 0.1 wt.% BTA + 1 wt.% NH_4OH slurry).

of oxide formation, removal and re-passivation. Following this repeated model, metal CMP could be controlled easily to achieve the global planarization. In the composition of urea–H_2O_2–BTA–NH_4OH, the adsorption of the BTA protects a concave from the wet etching and the formation of the native oxide can avoid the plastic deformation. Meanwhile, the passive film is formed in the alkaline urea–H_2O_2 slurry and the abraded oxide can be chelated by NH_3 rapidly.

3.4. Surface profile

Fig. 11 exhibits the AFM investigation of Cu surfaces. The rms-roughness (R_q) of Cu surfaces calculated by software package was used to compare the surface quality. It can be seen from Fig. 11(a) that the image of the Cu surface before CMP is the roughest and the calculated R_q is 68.761 nm for the scan size 5 µm × 5 µm. However, the Cu surface becomes smooth with the lower R_q after CMP by use of

5 wt.% urea–H_2O_2 slurries, and their AFM images are shown in Fig. 11(b)–(e). It is found that adding 0.1 wt.% BTA into 5 wt.% urea–H_2O_2 slurries could improve the planarization and its R_q decreased from 6.748 to 3.671 nm for the scan size 5 μm × 5 μm. However, adding 1 wt.% NH_4OH into 5 wt.% urea–H_2O_2 system made an increase in R_q from 6.748 to 26.646 nm. When 0.1 wt.% BTA and 1 wt.% NH_4OH were both added into 5 wt.% urea–H_2O_2 slurry, R_q decreased again even to 2.636 nm for the same scan size and an extremely smooth surface could be achieved, as shown in Fig. 11(e).

If the different degrees of Cu surface roughness and the non-uniform distribution of passive film are concerned, the impedance for the Cu–slurry interface usually exhibits a non-semicircular response for Nyquist plots. As a result, only a constant-phase element (CPE) instead of the ideal capacitance could fit the EIS results more agreeably. This constant-phase element (CPE) can be used to study the practical electrode with the different degrees of surface roughness, physical non-uniformity or a non-uniform distribution of surface reaction sites [23–25]. The impedance of the CPE is written as [25]

$$Z_{CPE} = [T(j\omega)^n]^{-1}$$

where T is a general admittance function; j, the complex operator $\sqrt{-1}$; and n, an adjustable parameter that usually lies between 0.5 and 1. The CPE describes an ideal capacitance with the high degree of planarization or homogeneities when $n = 1$. For the case of $n = 0.5$, an impedance relation, known as the Warburg impedance, is applicable; this impedance is associated with concentration and diffusion-related processes. Generally, the deviation from the ideal surface film capacitor can be estimated by this adjustable parameter. As listed in Table 3, it is worthy noting that the adjustable parameters of the double-layer CPE (n_{dl}) were dependent on the surface roughness of Cu no matter abrasion and no abrasion. Those adjustable parameters of the passive-film CPE (n_{pf}), however, remained smaller. It appears that the double layer is located at the Cu surface and its ideal performance of capacitance is controlled by the smooth Cu surface. Meanwhile, the smaller value of n_{pf} is due to the non-uniform corrosion on Cu surface and the brittleness of the passive film. From the comparison of n_{dl} between abrasion and no abrasion, it is clear that CMP helps the double-layer capacitance planar and the n_{dl} of abrasion would approach to 1. Especially, the n_{dl} of Cu after CMP using 5 wt.% urea–H_2O_2 + 0.1 wt.% BTA + 1 wt.% NH_4OH slurry was equal to 1, representing an ideal surface. These results are consistent with the AFM images mentioned earlier. Therefore, it is supposed that a smooth and homogeneous surface after Cu CMP can be obtained by use of the mixed slurry of urea–H_2O_2, BTA and NH_4OH, which is very adequate for delineation Cu patterns in the deep sub-micron integrated circuits.

Table 3
The adjusted parameters (n_{pf} and n_{dl}) of non-ideal double-layer capacitance and passive film capacitance and the surface roughness of copper corresponding the AFM images (Fig. 11) in various slurries

Slurry	No abrasion		Abrasion		R_q (nm)
	n_{pf}	n_{dl}	n_{pf}	n_{dl}	
5 wt.% urea–H_2O_2	0.77	0.90	0.81	0.91	6.748
5 wt.% urea–H_2O_2 + 0.1 wt.% BTA	–	0.87	–	0.95	3.671
5 wt.% urea–H_2O_2 + 1 wt.% NH_4OH	0.60	0.60	0.62	0.78	26.646
5 wt.% urea–H_2O_2 + 0.1 wt.% BTA +1 wt.% NH_4OH	0.58	0.90	0.58	1.00	2.636

4. Conclusions

This paper has presented the EIS results accompanied with the simulated equivalent circuit of double-capacitance mode for Cu in various urea–H_2O_2 slurries. The effects of different additives on the removal mechanism of Cu have also been analyzed and discussed. The results indicate that urea–H_2O_2 owns the high oxidizing ability with Cu and may act as a more stable oxidant to form an abradable passive film during CMP. Adding BTA into urea–H_2O_2 slurry may result in an efficient inhibition of the oxidation and etching on Cu while adding NH_4OH seems to enhance the dissolution and the oxidization rates substantially. Thus, electrochemical data indicate that combining both BTA and NH_4OH with urea–H_2O_2 slurry, the formation and removal of an abradable film could be controlled well during Cu CMP based on the repeated

mechanisms [3]. The contribution of each component in the slurry has been demonstrated by the measured corrosion parameters. Furthermore, it is worthy noting that the adjustable parameter of the double-layer CPE was dependent on the surface roughness of Cu. It could be an important indicator of CMP performance. AFM images indicate the surface characteristics of polished Cu agree well with the discussion of the EIS results. Fewer micro-scratches and more global planarization were observed for Cu CMP using 5 wt.% urea–H_2O_2 + 0.1 wt.% BTA + 1 wt.% NH_4OH slurry. The EIS measurement may be useful in providing the electrochemical information of metal CMP in various slurries and in choosing the appropriate composition from large number of chemicals for CMP use.

Acknowledgements

The authors would like to thank the National Science Council in Taiwan for financially supporting this research under Contract no. NSC 90-2214-E-002-008.

References

[1] D. Edelstein, J. Heidenreich, R. Goldblatt, W. Cote, C. Uzoh, N. Lustig, P. Roper, T. McDevitt, W. Motsiff, A. Simon, J. Dukovic, R. Wachnik, H. Rathore, R. Schulz, S. Su, S. Luce, J. Diggest, in: Proceedings of the International Conference IEEE International on Electron Devices Meeting, Washington, DC, 1997, p. 773.
[2] W.F. Smith, Foundations of Materials Science and Engineering, 2nd ed., McGraw-Hill Inc., New York, 1994 (Chapter 5).
[3] F.B. Kaufman, D.B. Thompson, R.E. Broadie, M.A. Jaso, W.L. Guthrie, D.J. Pearson, M.B. Small, J. Electrochem. Soc. 138 (1991) 3460–3465.
[4] R. Carpio, J. Farkas, R. Jairath, Thin Solid Films 266 (1995) 238–244.
[5] Y. Gotkis, S. Alamgir, L. Yang, F. Dai, F. Mitchell, J. Nguyen, L. Shumway, L.R. Walesa, J. Yang, P. Nunan, K. Holland, J. Vacuum Soc. Technol. B 17 (1999) 2269–2271.
[6] P. Wrschka, J. Hernandez, G.S. Oehrlein, J.A. Negrych, G. Haag, P. Rat, J.E. Currie, J. Electrochem. Soc. 148 (2001) G321–G325.
[7] Y. Li, S.V. Babu, Electrochem. Solid-State Lett. 4 (2001) G20–G22.
[8] T.H. Tsai, S.C. Yen, in: Proceedings of the 199th Electrochemical Society Meeting, Washington, DC, 2001.
[9] V. Nguyen, H. VarKranenburg, P. Woerlee, Microelectron. Eng. 50 (2000) 403–410.
[10] J.M. Steigerwald, D.J. Duquette, S.P. Murarka, R.J. Gutmann, J. Electrochem. Soc. 142 (1995) 2379–2385.
[11] H.G. Kim, Y.M. An, D.K. Moon, J.G. Park, Jpn. J. Appl. Phys. 39 (3A) (2000) 1085–1090.
[12] W.C. Chen, C.T. Yen, J. Vacuum Soc. Technol. B 18 (2000) 201–207.
[13] M.T. Wang, M.S. Tsai, C. Liu, W.T. Tseng, T.C. Chang, M.C. Chen, Thin Solid Films 308–309 (1997) 518–522.
[14] T.C. Hu, S.Y. Chiu, B.T. Dai, M.S. Tsai, I.C. Tung, M.S. Feng, Mater. Chem. Phys. 61 (1999) 169–171.
[15] L. Zang, S. Raghavan, M. Weling, J. Vacuum Soc. Technol. B 17 (1999) 2248–2255.
[16] T.H. Tsai, S.C. Yen, in: Proceedings of the Fifth International Symposium in 201st Electrochemical Society Meeting on Chemical Mechanical Polishing (CMP), Philadelphia, PA, 2002.
[17] J.R. Scully, D.C. Silverman, M.W. Kendig, Electrochemical Impedance: Analysis and Interpretation, ASTM Publication, Philadelphia, 1993.
[18] H.S. Kuo, W.T. Tsai, Mater. Chem. Phys. 69 (2001) 53–61.
[19] D.A. Jones, Principles and Prevention of Corrosion, 2nd ed., Prentice Hall, Upper Saddle River, NJ, 1983.
[20] E. Stupnisek-Lisac, V. Cinotti, D. Reichenbach, J. Appl. Electrochem. 29 (1999) 117–122.
[21] M. Pourbaix, Atlas of Electrochemical Equilibria in Aqueous Solutions, NACE, Houston, TX, 1975.
[22] C.E. Mortimer, Chemistry, Wadsworth Publication Co., Belmont, CA, 1983, pp. 371–427.
[23] Y. Choquette, A. Lasia, L. Brossard, H. Menard, J. Electrochem. Soc. 137 (1990) 1723.
[24] A.J. Griffin Jr., F.B. Brotzen, J. Electrochem. Soc. 141 (1994) 3473–3479.
[25] R. Babic, M. Metikos-Hukovic, A. Jukic, J. Electrochem. Soc. 148 (2001) B146–B151.